Nonlinear frequency conversion with quasi-phase-mismatch effect

Hongchen Guo, Sing Hai Tang, and Yiqiang Qin
Department of Physics, National University of Singapore, 117542, Singapore

Yong Yuan Zhu
National Laboratory of Solid State Microstructures, Nanjing University, Nanjing, 210093, People's Republic of China
(Received 21 December 2004; published 29 June 2005)

In conventional frequency conversion based on $\chi^{(2)}$-induced nonlinear optical effects, a number of phase-matching techniques have been deployed to resolve the phase mismatch between the interacting waves. In this work, we report that in the quasi-phase-matching scheme, the accumulation of the phase mismatch can induce a quasi-phase-mismatch effect. And on the contrary, instead of eliminating the phase mismatch, modulating the quasi-phase-mismatch effect can lead to bandwidth enhancement and multiple-wavelength conversion. Both of these are essential factors for applications in nonlinear frequency conversion. As examples, designs with reset-periodic and cascaded-periodic optical superlattices based on such modulation are presented.

DOI: 10.1103/PhysRevE.71.066615 PACS number(s): 42.70.Mp, 42.65.Ky, 77.84.−s

I. INTRODUCTION

One of the most striking events in condensed-matter physics in recent years is the investigation of the interactions between wave vectors of classical waves and reciprocal vectors of artificial optical superlattices. In the quasi-phase-matching (QPM) scheme of nonlinear optics, the interactions have led to laser frequency generation and conversion with periodically poled [1] ferroelectric crystals such as $LiNbO_3$ [2], $LiTaO_3$ [3], and $KTiOPO_4$ [4]. These laser frequency generations and conversions are attractive sources of coherent radiation for applications where laser sources were hitherto unavailable or a wide bandwidth and tunable range was needed. In the past ten years, QPM was introduced into nonlinear optics as an alternative technique to birefringence phase matching (BPM). QPM has advantages over BPM due to its higher gain, no "walk-off," greater allowance for noncritical phase matching of interactions within the transparency range, lower sensitivity to photorefractive effects [5], and extended ir transmission [6].

In the periodic optical superlattice (POSL), QPM is achieved by offsetting the wave vector mismatch between the interacting waves via the reciprocal vectors of the superlattice. However, phase mismatch is a ubiquitous effect since any experimental uncertainty, such as the nonideal nature of the domain inversion, a variation of the superlattice length during the poling process, the fluctuation of the cavity and the pump source, will result in an additional phase mismatch in the superlattice. On the other hand, this additional phase mismatch is an essential factor related to the requirement of wide bandwidth and tuning, as well as the cascaded nonlinear interactions [7,8]. The accumulation of this additional phase mismatch in the POSL will induce a quasi-phase-mismatch (QPMM) effect. Until now, much effort has been devoted to developing the QPM technique in various optical superlattices [9–15], whereas the study of the QPMM effect has so far been overlooked. In this paper, the QPMM effect in ferroelectric optical superlattices is investigated. Effective modulations of QPMM by microstructural designs can result in bandwidth enhancement and multiple-wavelength output in $\chi^{(2)}$-induced frequency conversion processes. Accordingly, this paper is organized as follows. In Sec. II, the QPMM effect in the conventional periodic superlattice is discussed. In Sec. III, the bandwidth enhancement by the modulation of the QPMM effect in a reset-periodic optical superlattice (RPOSL) is presented. In Sec. IV, the multiple-wavelength conversion by the modulation of the QPMM effect in the cascaded-periodic optical superlattice (CPOSL) is presented. Finally, in Sec. V, the conclusions are presented.

II. QPMM EFFECT IN THE CONVENTIONAL POSL

A. First-order QPM condition in POSL

Normally, only the first-order QPM condition [9] is employed to compensate the wave vector mismatch for the designed wavelength. For example, consider the nonlinear difference frequency mixing (DFM) process. Under the first-order QPM condition, the wave vector mismatch of the pump, input signal, and converted output beams is compensated by the reciprocal vector of the superlattice defined by $2\pi/\Lambda_0$, where Λ_0 is the period of the first-order QPM superlattice. Under the plane wave approximation and the slowly varying envelope approximation, the coupling equations are given by

$$\frac{dE_p(x)}{dx} = \frac{-i\omega_p d_{\text{eff}} f(x)}{n_p c} E_s(x) E_{\text{out}}(x) \exp(i\Delta k x),$$

$$\frac{dE_s(x)}{dx} = \frac{-i\omega_s d_{\text{eff}} f(x)}{n_s c} E_p(x) E_{\text{out}}{}^*(x) \exp(-i\Delta k x),$$

$$\frac{dE_{\text{out}}(x)}{dx} = \frac{-i\omega_{\text{out}} d_{\text{eff}} f(x)}{n_{\text{out}} c} E_p(x) E_s{}^*(x) \exp(-i\Delta k x), \quad (1)$$

where $n_p, n_s, n_{\text{out}}, \omega_p, \omega_s$, and ω_{out} represent the refractive index and angular frequency of the pump, signal, and output beams, respectively. c is the speed of light in vacuum, and d_{eff} is the effective second-order nonlinearity. $f(x)$ is the spa-

tial function that modulates the sign of d_{eff} in the superlattice and is defined by

$$f(x) = 1 - 2\text{int}\left(\frac{2x}{\Lambda_0}\right) + 4\text{int}\left(\frac{x}{\Lambda_0}\right) \tag{2}$$

where int(x) takes the value of the largest integer $\leqslant x$. The spatial function $f(x)$ only takes the values $+1$ or -1 that represent the two inverse polarization directions in ferroelectric materials.

In our discussion, pump depletion is taken into account in order to keep a universal appeal and the coupling equations are numerically solved. As shown in Fig. 1(a), when the first-order QPM condition is satisfied, the direction of spontaneous polarization flips over at every coherence length $l_{c_0} = \pi/\Delta k_0$, i.e., the distance over which the relative phase of the three waves changes by π. Likewise the intensity of the output beam increases stepwise at every coherent length.

B. QPMM effect in POSL

When there is additional phase mismatch, the QPM condition will be disturbed by a factor of $\delta_{\Delta k}$, which is defined by

$$\delta_{\Delta k} = k_p - k_s - k_{\text{out}} - \Delta k_0 = \Delta k - \Delta k_0 = \Delta k - \frac{2\pi}{\Lambda_0}. \tag{3}$$

As shown in Fig. 1(b), the flip over of the spontaneous polarization in the original superlattice fails to match to the new coherence length $l_c = \pi/\Delta k = \pi/(\delta_{\Delta k} + \Delta k_0)$. This will reduce the efficiency compared to the situation of perfect QPM condition. However, the output intensity still increases stepwise until $\delta_{\Delta k}$ accumulates to π as shown in Fig. 1(c). Thus we can define a coherence length appropriately named the QPMM coherence length l_c^{QPMM}, to account for this additional phase mismatch $\delta_{\Delta k}$:

$$l_c^{\text{QPMM}} = \pi/|\delta_{\Delta k}|. \tag{4}$$

l_c^{QPMM} thus determines a part of the crystal in which the interacting waves with $\delta_{\Delta k}$ can be still efficiently quasi-phase-matched and the output intensity increases stepwise until the wave has traveled a distance of l_c^{QPMM}.

Based on the QPMM effect, there are two types of domain structural modulation that can be introduced: one for bandwidth widening with a RPOSL, and the other for multiple-wavelength conversion with a CPOSL. The details of the modulations are described in the following sections.

III. MODULATION OF QPMM IN RPOSL

A. Reset and bandwidth enhancement

One of the most important technologies of nonlinear optical wavelength mixing is the ability to enhance the bandwidth. In this part, we present an effective bandwidth enhancement in the light of modulating the QPMM effect in a RPOSL. Due to the QPMM effect, the output intensity begins to decrease when $\delta_{\Delta k}$ has accumulated to π after a distance l_c^{QPMM}. However, as in QPM, it is possible for the intensity to continue to increase further if the accumulated phase mismatch π at l_c^{QPMM} can be reset. The reset action, which is equivalent to superimposing an additional domain reversal on the original POSL [Fig. 2(a)], will modify the structure of it and cause each of the subsequent domains to reverse its original polarization direction as shown in Fig. 2(b). Not only will this reset action cause the continuous increase of the spectral component of $\delta_{\Delta k}$, but it will further affect all the other spectral components, causing those spectral components with phase mismatches smaller than $\delta_{\Delta k}$ (larger l_c^{QPMM}) to lower output intensities while those with phase mismatches larger than $\delta_{\Delta k}$ (smaller l_c^{QPMM}) increase their output intensities. The net effect of intensity redistribution therefore results in an enhancement of bandwidth.

We consider the bandwidth enhancement in the nonlinear DFM process. The wavelengths of the pump, input signal, and converted output beams are chosen to be $\lambda_p = 775$ nm, $\lambda_s = 1545$ nm, and $\lambda_{\text{out}} = 1555$ nm to fit the optical communication window. A 15-mm-long $LiNbO_3$ crystal is taken as an example. The first-order QPM period is calculated to be $\Lambda_0 = 16.92$ μm based on the Sellmeier coefficients [16] at room temperature, and the wave vector mismatch of the designed wavelengths is $\Delta k_0 = 2\pi/\Lambda_0 = 0.3713$ μm^{-1}.

B. Reset position

The most important factor in designing the RPOSL is the determination of the reset position (denoted by L_{reset}) to effectively modulate all the spectral components for a given bandwidth requirement. Normally, the proper L_{reset} can be determined via analytically solving the coupling equations to obtain the relationship between power and the variables L_{reset} and $\delta_{\Delta k}$. But this approach requires the small signal approximation, which is no longer tenable in our discussion. And since a transcendental equation is obtained (see the Appendix), the final determination of the proper reset position will depend on a numerical balancing process similar to that discussed here. Considering the fact that the Fourier spectrum is similar to the power spectrum of the frequency difference output, a Fourier analysis is adopted in our calculation. First the Fourier transform of the domain sequence is performed. Then the proper value of L_{reset} is obtained through a numerical balancing process, resulting in a wideband Fourier spectrum. Finally, the Fourier spectrum is converted to the power spectrum via the coupling equations.

To perform the Fourier analysis, we define first the spatial function that describes the domain sequence of the RPOSL in real space. As described above, when a reset is superimposed, the part in front of the reset [denoted by L_1 in Fig. 2(b)] retains its original domain orientations, whereas the rear part [denoted by L_2 in Fig. 2(b)] has its polarization directions completely reversed. Thus the spatial function is discontinuous. For example, for the RPOSL with one reset superimposed, the spatial function is given by

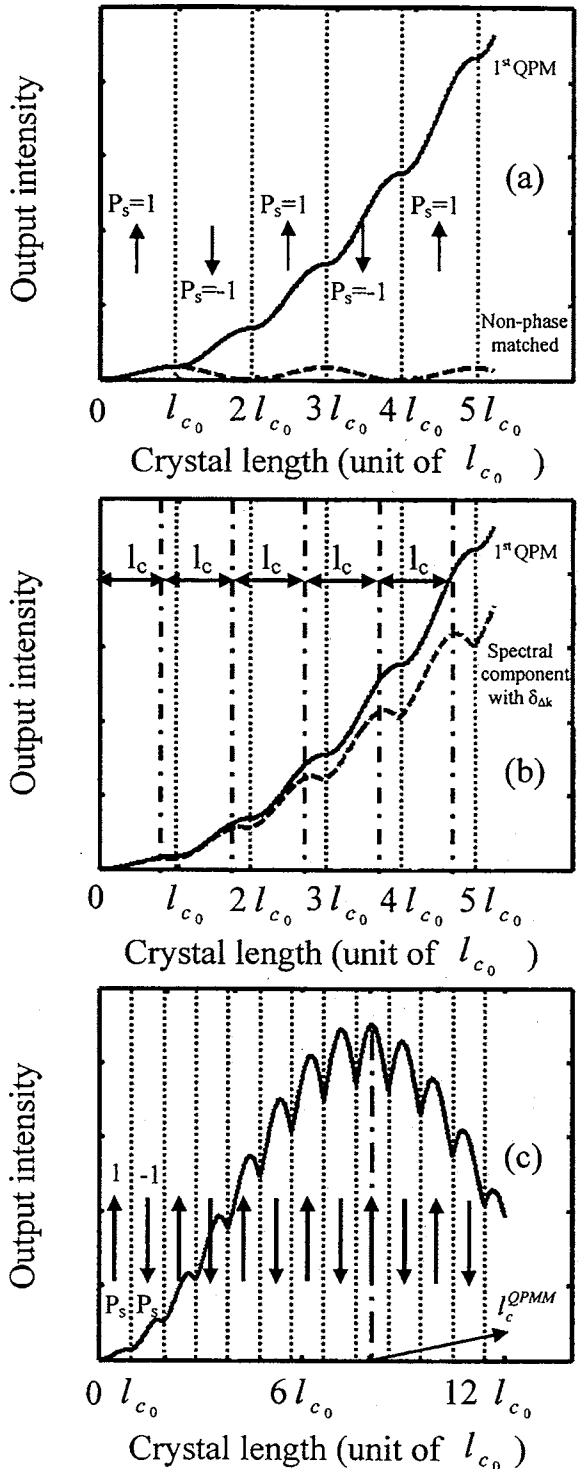

FIG. 1. (a) Effect of QPM on the growth of intensity with distance in a POSL. The direction of spontaneous polarization flips every coherence length. Solid curve for first-order QPM; dashed curve for non-phase-matched interaction. (b) Effect of the additional phase mismatch $\delta_{\Delta k}$ in the POSL. Solid curve for first-order QPM; dashed curve for spectral component with $\delta_{\Delta k}$. It is seen that the flip over of the spontaneous polarization in the POSL fails to match the new coherence length l_c. (c) Within l_c^{QPMM}, the spectral component with $\delta_{\Delta k}$ can be still efficiently quasi-phase-matched, i.e., the output intensity retains a stepwise increase until it reaches the coherence length l_c^{QPMM}.

$$f_1(x) = 1 - 2\mathrm{int}\left(\frac{2x}{\Lambda_0}\right) + 4\mathrm{int}\left(\frac{x}{\Lambda_0}\right), \quad x \in [0, L_1],$$

$$f_2(x) = (-1)\left[1 - 2\mathrm{int}\left(\frac{2x}{\Lambda_0}\right) + 4\mathrm{int}\left(\frac{x}{\Lambda_0}\right)\right], \quad x \in (L_1, L_{\mathrm{sup}}], \tag{5}$$

where L_{sup} is the entire length of the RPOSL. Applying the Fourier transform

$$\begin{aligned} F(\Delta k) &= \frac{1}{L_{\mathrm{sup}}}\int_0^{L_{\mathrm{sup}}} f(x)\exp(-i\Delta k x)dx \\ &= \frac{1}{L_{\mathrm{sup}}}\left[\int_0^{L_1} f_1(x)\exp(-i\Delta k x)dx \right. \\ &\quad \left. + \int_{L_1}^{L_{\mathrm{sup}}} f_2(x)\exp(-i\Delta k x)dx\right], \end{aligned} \tag{6}$$

one can obtain the expression of $F(\Delta k)$ in terms of $\delta_{\Delta k}$.

$$\begin{aligned} F(\Delta k) = \frac{1}{L_{\mathrm{sup}}}\Bigg[& \sum_{m=0}^{L_1/\Lambda_0-1} \int_{2m\Lambda_0/2}^{(2m+1)\Lambda_0/2} \exp(-i\Delta k_0 x) \\ & \times \exp(-i\delta_{\Delta k}x)dx - \sum_{m=0}^{L_1/\Lambda_0-1} \int_{(2m+1)\Lambda_0/2}^{(2m+2)\Lambda_0/2} \exp(-i\Delta k_0 x) \\ & \times \exp(-i\delta_{\Delta k}x)dx - \sum_{m=L_1/\Lambda_0}^{L_{\mathrm{sup}}/\Lambda_0-1} \int_{(2m)\Lambda_0/2}^{(2m+1)\Lambda_0/2} \exp(-i\Delta k_0 x) \\ & \times \exp(-i\delta_{\Delta k}x)dx + \sum_{m=L_1/\Lambda_0}^{L_{\mathrm{sup}}/\Lambda_0-1} \int_{(2m+1)\Lambda_0/2}^{(2m+2)\Lambda_0/2} \exp(-i\Delta k_0 x) \\ & \times \exp(-i\delta_{\Delta k}x)dx\Bigg]. \end{aligned} \tag{7}$$

After a series of deductions where $2L_1/\Lambda_0 \gg 1$ and $2L_{\mathrm{sup}}/\Lambda_0 \gg 1$, we obtain

$$\begin{aligned} F(\Delta k) = \frac{2}{i\Delta k L_{\mathrm{sup}}\Lambda_0}\left[\exp\left(-i\delta_{\Delta k}\frac{\Lambda_0}{2}\right) + 1\right] \\ \times\left[\int_0^{L_1}\exp(-i\delta_{\Delta k}x)dx - \int_{L_1}^{L_{\mathrm{sup}}}\exp(-i\delta_{\Delta k}x)dx\right]. \end{aligned} \tag{8}$$

The integration is carried out with $\delta_{\Delta k} \ll \Delta k_0$. The spectrum intensity, i.e., the Fourier coefficient, is given approximately by

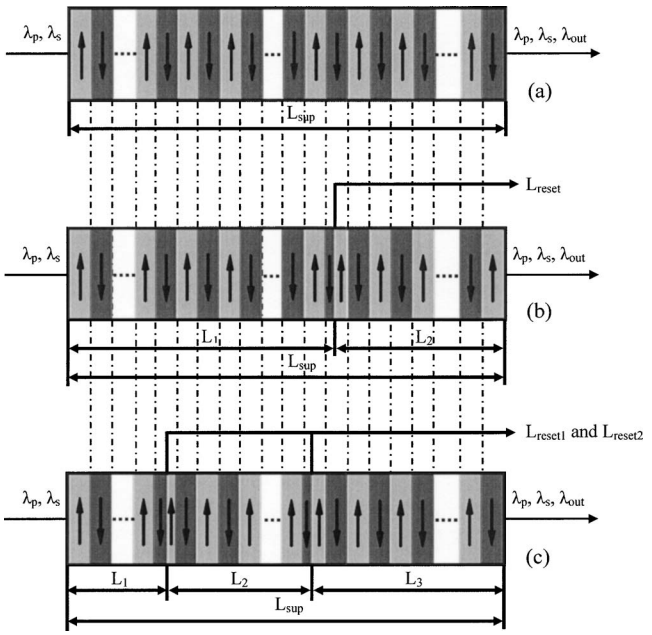

FIG. 2. (a) Schematic diagram of a POSL. (b) Schematic diagram of a RPOSL with one reset. (c) Schematic diagram of a RPOSL with two resets. The arrows show the directions of spontaneous polarization of ferroelectric materials.

$$|F(\Delta k)| \approx \frac{4}{\Delta k \delta_{\Delta k} \Lambda_0 L_{\mathrm{sup}}} \left[2 \sin^2\left(\frac{\delta_{\Delta k} L_1}{2} \right) + 2 \sin^2\left(\frac{\delta_{\Delta k}(L_{\mathrm{sup}} - L_1)}{2} \right) - \sin^2\left(\frac{\delta_{\Delta k} L_{\mathrm{sup}}}{2} \right) \right]^{1/2}. \tag{9}$$

It is clear that the combination of several sinusoidal terms with different widths and amplitudes will result in an enlarged bandwidth. However, Eq. (9) is a transcendental equation where the two variables $\delta_{\Delta k}$ and L_1 are coupled to each other in sinusoidal functions. The determination of the reset position L_1 (i.e., L_{set}) is seen to be a balancing act of three competing factors: the full width at half maximum (FWHM) of the Fourier spectrum (related to bandwidth), the spectrum intensity of the central spectral component (related to conversion efficiency), and the smoothness of the spectrum around the central spectral component Δk_0 (related to effectivity). As shown in Fig. 3(a), the FWHM of the spectrum is not necessarily wide if the spectrum intensity is overvalued. Equally important is the smoothness of the spectrum around the central spectral component. As shown in Fig. 3(b), the spectrum is so uneven around Δk_0 that it renders the RPOSL unsuitable for practical applications.

All the three factors are considered in the following sequence. First, all the possible combinations are scanned, i.e., L_1 changes from 0 to L_{sup} and $L_2 = L_{\mathrm{sup}} - L_1$. Then for each combination, the Fourier spectrum is obtained from Eq. (9) by scanning $\delta_{\Delta k}$ over a wide range of values and the value at half maximum is computed to ensure the desired output conversion efficiency (normally $\geqslant 0.15$). Simultaneously, the smoothness of the spectrum around the central spectral component is controlled by adjusting the difference between the value of the Fourier coefficients at the point $\delta_{\Delta k} = 0$ and the global maximum value. Our numerical interation process shows that the optimized reset position is 12.3 mm for a 15-mm-long superlattice, as shown in Fig. 3(c). Furthermore, on converting the Fourier spectrum into the power spectrum, it is seen that the bandwidth of the RPOSL (dotted curve in Fig. 4) becomes wider compared to that of the POSL (solid curve in Fig. 4). The FWHM of the dotted curve is more than twice larger than that of the solid curve.

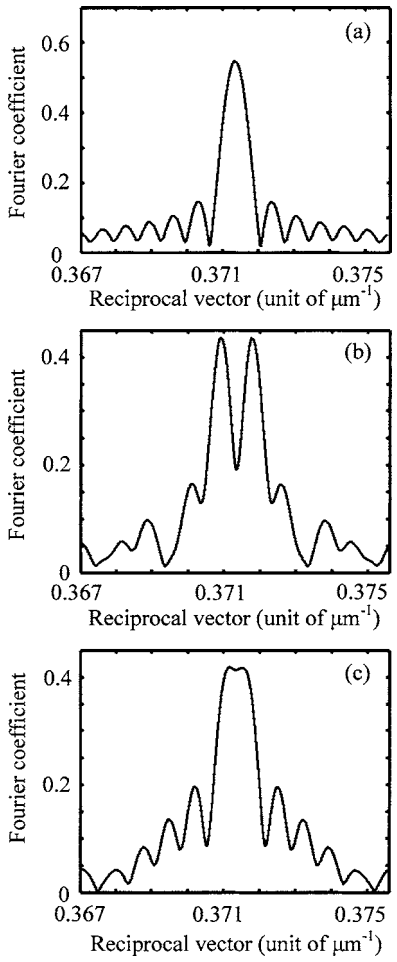

FIG. 3. Fourier spectrum of a RPOSL with one reset. (a) The spectrum intensity of the central spectral component is overvalued during the numerical balance process. Thus the enhancement of the spectrum bandwidth is not necessarily efficient. (b) The spectrum around the central spectral component varies sharply. It renders the RPOSL unsuitable for practical applications. (c) After balancing the three factors, the FWHM of the Fourier spectrum, the spectrum intensity of the central spectral component, and the smoothness of the spectrum around the central spectral component, effective bandwidth enhancement of the Fourier spectrum is achieved.

In adopting the method of Fourier analysis, we have avoided solving the complex coupling equations. It provides a more general approach to effectively achieve bandwidth enhancement with or without small signal approximation. Furthermore, for the RPOSL with two resets superimposed as shown in Fig. 2(c), the spectrum intensity shows a combination of more sinusoidal terms as expressed by

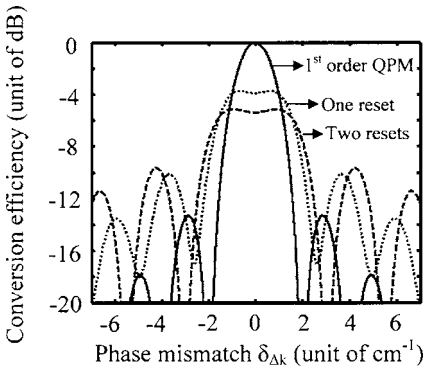

FIG. 4. Comparison of the tuning curve between the POSL (solid curve) and the RPOSL with one (dotted curve) and two resets (dashed curve). The conversion efficiency is the relative conversion efficiency and is normalized to the peak efficiency. It is seen that more resets are superimposed, wider bandwidth and smaller efficiency are obtained. That is, an inevitable trade-off exists between bandwidth and conversion efficiency.

$$|F(\Delta k)| \approx \frac{4}{\Delta k \delta_{\Delta k} \Lambda_0 L_{\sup}} \left[2 \sin^2\left(\frac{\delta_{\Delta k} L_1}{2}\right) + 4 \sin^2\left(\frac{\delta_{\Delta k} L_2}{2}\right) + 2 \sin^2\left(\frac{\delta_{\Delta k}(L_{\sup} - L_1 - L_2)}{2}\right) - 2 \sin^2\left(\frac{\delta_{\Delta k}(L_1 + L_2)}{2}\right) - 2 \sin^2\left(\frac{\delta_{\Delta k}(L_{\sup} - L_1)}{2}\right) + \sin^2\left(\frac{\delta_{\Delta k} L_{\sup}}{2}\right) \right]^{1/2}. \quad (10)$$

The two reset positions (L_1 and L_2) for effective bandwidth enhancement are around 1.8 and 11.55 mm, respectively, after a similar numerical computation. Comparing the solid curve with the dotted curve and the dashed curve in Fig. 4, it is seen that when more resets are superimposed, a wider bandwidth with lower efficiency is obtained. It is easy to understand from the point of view of the Fourier theorem: Perturbing the periodic structure will naturally result in a broadened spectrum. However, the Fourier coefficients of the reciprocal vector $2\pi/\Lambda_0$ will be reduced due to the inevitable trade-off that exists between bandwidth and conversion efficiency.

IV. MODULATION OF QPMM IN CPOSL

A. Cascaded modulations for conversion of even number of wavelengths

Besides the bandwidth enhancement, multiple-wavelength conversion is another important aspect in nonlinear optical mixing. It is essential for many applications such as environmental sensing, gas detection, wavelength-division-multiplexes optical communication networks, and signal processing in time-division-multiplexed systems. Here we present an approach for efficient multiple-wavelength operation by modulating the QPMM in a CPOSL.

In analogy to the QPM where the period for the QPM is given by $\Lambda_0 = 2l_{c_0}$, the modulation period $\Lambda = 2l_c^{\mathrm{QPMM}}$ is similarly defined for the QPMM effect. Furthermore, multiple-wavelength conversion can be realized if a number of modulation periods are defined and combined in a CPOSL design. For simplicity, a CPOSL [Fig. 5(a)] is described by considering the following case. A POSL with period Λ_0 as determined by the central wavelength and total length $L_{\sup}$ is divided into N equal segments. On each segment, a new periodic structure with a different modulation period ($\Lambda_{mn} = 2l_{c(\delta_{\Delta kn})}^{\mathrm{QPMM}}$, $n \in [1, N]$) is superimposed. Thus a spectral component with a phase mismatch $\delta_{\Delta k}$ (determined by the requirement of the output wavelength) can be efficiently generated at each of the segmented superlattices. As seen from Eq. (4), $\delta_{\Delta k} = \pm \pi / l_c^{\mathrm{QPMM}}$; thus N different modulation periods can modulate a total of $2N$ additional phase mismatches which denote by $\pm\delta_{\Delta k_1}, \pm\delta_{\Delta k_2}, \pm\delta_{\Delta k_3}, \ldots, \pm\delta_{\Delta k_N}$. As each segmented superlattice has equal length, all $2N$ wavelengths distributed symmetrically around the central wavelength will have roughly the same efficiency.

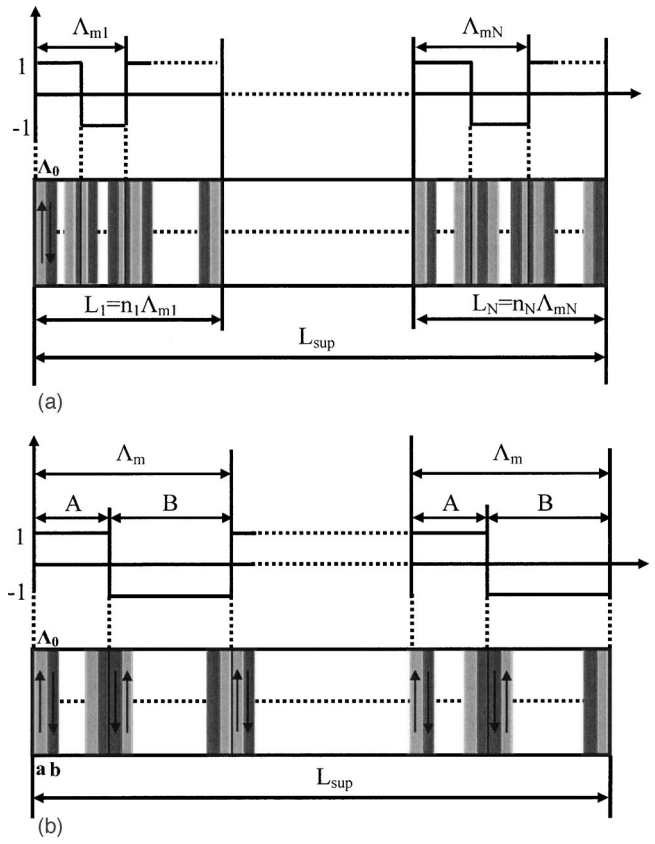

FIG. 5. (a) Schematic illustration of a CPOSL superimposed by N modulation periods, where $n_1, \ldots, n_N$ are integers. (b) Schematic diagram of a CPOSL superimposed by one modulation period. The duty cycles of the original period Λ_0 and the modulation period Λ_m can be adjusted. The arrows show the directions of spontaneous polarization of ferroelectric materials.

The spatial function for the entire CPOSL can be expressed discontinuously. In each segmented superlattice, the spatial distribution of the effective nonlinearity is described by combining the two spatial terms [Eq. (2)] for Λ_m and Λ_0. Thus in the entire length of the superlattice, we obtain

$$
\begin{aligned}
f_1(x) &= \left[1 - 2\mathrm{int}\left(\frac{2x}{\Lambda_{m1}}\right) + 4\mathrm{int}\left(\frac{x}{\Lambda_{m1}}\right)\right]\left[1 - 2\mathrm{int}\left(\frac{2x}{\Lambda_0}\right) + 4\mathrm{int}\left(\frac{x}{\Lambda_0}\right)\right], \quad x \in [0, L_1], \\
f_2(x) &= \left[1 - 2\mathrm{int}\left(\frac{2x}{\Lambda_{m2}}\right) + 4\mathrm{int}\left(\frac{x}{\Lambda_{m2}}\right)\right]\left[1 - 2\mathrm{int}\left(\frac{2x}{\Lambda_0}\right) + 4\mathrm{int}\left(\frac{x}{\Lambda_0}\right)\right], \quad x \in (L_1, L_1 + L_2], \\
&\vdots \\
f_N(x) &= \left[1 - 2\mathrm{int}\left(\frac{2x}{\Lambda_{mN}}\right) + 4\mathrm{int}\left(\frac{x}{\Lambda_{mN}}\right)\right]\left[1 - 2\mathrm{int}\left(\frac{2x}{\Lambda_0}\right) + 4\mathrm{int}\left(\frac{x}{\Lambda_0}\right)\right], \quad x \in (L_1 + \cdots + L_{N-1}, L_{\mathrm{sup}}].
\end{aligned}
\tag{11}
$$

For example, our simulation of a 20-mm-long superlattice with $\Lambda_0 = 16.92\ \mu$m is divided into two equal segmented superlattices. Two modulation periods $\Lambda_{m1} = 676.8\ \mu$m and $\Lambda_{m2} = 1692\ \mu$m are superimposed on the two segmented superlattices. According to the analysis above, there are four peaks with almost equal height in the Fourier spectrum [Fig. 6(a)] and power spectrum [Fig. 6(b)]. Similarly, multiwavelength operation with more channels and different channel spacing can also be achieved by adopting this design.

B. Duty cycle of the modulation period for conversion of odd number of wavelengths

It is seen in the aforementioned modulation of the QPMM effect that the central wavelength is always absent and thus we can only obtain an even number of wavelength outputs. In this section, this phenomenon is discussed from a more general perspective in which both duty cycles Λ_0 and Λ_m can be adjusted.

For simplicity, we consider the case in which only one modulation periodicity is superimposed on a POSL, as shown in Fig. 5(b). The original POSL with period Λ_0 is chosen to compose of length L_{sup} with duty cycle D_0. Thus the entire superlattice consists of two types of domains: the a domain with a width of $a = \Lambda_0 D_0$ and a b domain with a width of $b = \Lambda_0 - \Lambda_0 D_0$. A modulation period Λ_m (defined by $\Lambda_m = 2l_c^{\mathrm{QPMM}} = 2\pi/\delta_{\Delta K}$) is superimposed on the POSL. The duty cycle of Λ_m is denoted by D_m, and thus the entire superlattice consists of two types of segments: the A segment with a length of $A = \Lambda_m D_m$ and a B segment with a length of $B = \Lambda_m - \Lambda_m D_m$.

$F(\Delta k)$ consists of contributions from both the a domain and the b domain, i.e.,

$$
F(\Delta k) = F_a(\Delta k) + F_b(\Delta k). \tag{12}
$$

Considering the fact that the a and b domains can be in different segments (A or B segment), Eq. (12) can be further expressed by

$$
\begin{aligned}
F(\Delta k) = F_a(\Delta k) + F_b(\Delta k) &= F_a^A(\Delta k) + F_a^B(\Delta k) + F_b^A(\Delta k) \\
&+ F_b^B(\Delta k).
\end{aligned}
\tag{13}
$$

For simplicity, we assume that the quotients of $L_{\mathrm{sup}}/\Lambda_0, L_{\mathrm{sup}}/\Lambda_m, \Lambda_m/\Lambda_0, A/\Lambda_0$, and B/Λ_0 are integers. Thus the four terms $F_a^A(\Delta k), F_a^B(\Delta k), F_b^A(\Delta k)$, and $F_b^B(\Delta k)$ in Eq. (13) can be analytically expressed by applying the Fourier transform:

$$
F_{a,b}^A(\Delta k) = \frac{S}{-i\Delta k L_{\mathrm{sup}}}[\exp(-i\Delta k\xi) - 1]\exp(-i\varepsilon\Delta k a)\frac{1 - \exp(-i\Delta k A)[1 - \exp(-i\Delta k j\Lambda_{\mathrm{mod}})]}{1 - \exp(-i\Delta k\Lambda_0)[1 - \exp(-i\Delta k\Lambda_{\mathrm{mod}})]},
$$

$$
F_{a,b}^B(\Delta k) = \frac{S}{i\Delta k L_{\mathrm{sup}}}[\exp(-i\Delta k\xi) - 1]\exp(-i\varepsilon\Delta k a)\frac{[1 - \exp(-i\Delta k B)]\exp(-i\Delta k A)[1 - \exp(-i\Delta k j\Lambda_{\mathrm{mod}})]}{1 - \exp(-i\Delta k\Lambda_0)[1 - \exp(-i\Delta k\Lambda_{\mathrm{mod}})]}. \tag{14}
$$

For the a domain, $\xi = a$, $\varepsilon = 0$, $S = 1$, and for the b domain, $\xi = b$, $\varepsilon = 1$, $S = -1$, where A, B, and Λ_m are defined by $A = p\Lambda_0$, $B = q\Lambda_0$, and $L_{\mathrm{sup}} = j\Lambda_m = j(p+q)\Lambda_0$ (p, q, and j are integers). The spectrum intensity of the central spectral component ($|F(\Delta k_0)|$) can finally be written as

$$
\left|\lim_{\Delta k \to \Delta k_0} F(\Delta k)\right| = \left|\frac{4\sin(\Delta k_0 a/2)}{\pi} D_m - \frac{2\sin(\Delta k_0 a/2)}{\pi}\right|. \tag{15}
$$

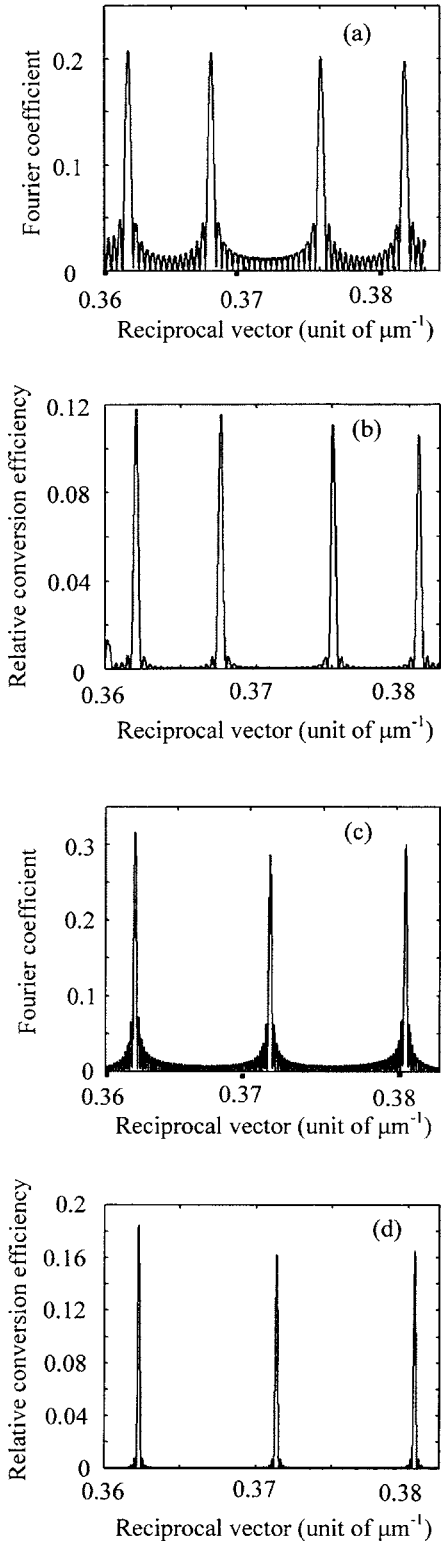

FIG. 6. (a) Four-channel Fourier spectrum of a CPOSL with two modulation periods superimposed. (b) Conversion efficiency plot of (a). The conversion efficiency is relative to the peak efficiency of a conventional POSL (one-channel) device. (c) Three-channel Fourier spectrum of a CPOSL with one modulation period superimposed. (d) Conversion efficiency plot of (c). The conversion efficiency is relative to the peak efficiency of a conventional POSL (one-channel) device.

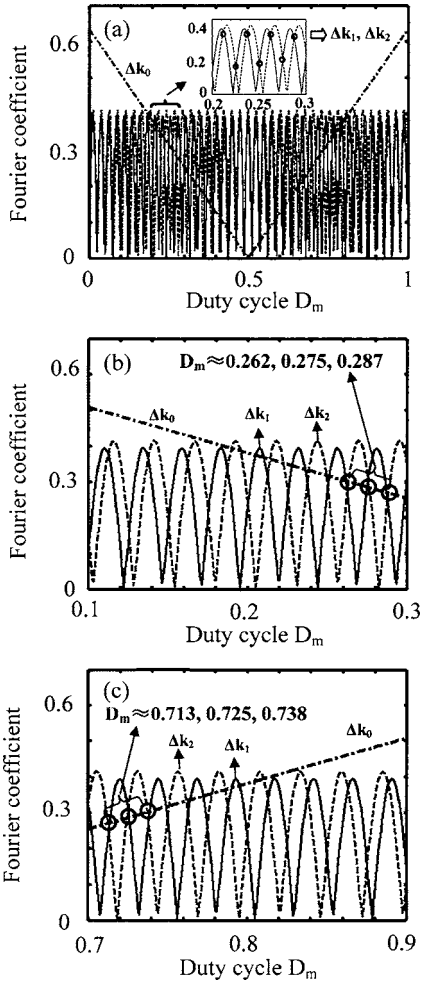

FIG. 7. (a) Distributions of $|F(\Delta k_0)|$, $|F(\Delta k_1)|$, and $|F(\Delta k_2)|$ as functions of D_m; dash-dotted curve for $|F(\Delta k_0)|$, solid curve for $|F(\Delta k_1)|$, and dashed curve for $|F(\Delta k_2)|$. $|F(\Delta k_1)|$ and $|F(\Delta k_2)|$ can be equalized at a series of discrete values of D_m as indicated by the black circles in the inset. (b),(c) When the values of D_m are around 0.262, 0.275, and 0.287 or $(1-0.262)$, $(1-0.275)$, and $(1-0.287)$, $|F(\Delta k_0)|$, $|F(\Delta k_1)|$, and $|F(\Delta k_2)|$ can be roughly equalized at the maximum value. Here, $\Lambda_m=676.8$ μm and $\Lambda_0=16.92$ μm.

It is seen that when the duty cycle D_m of the modulation period is set to be 50%, $|F(\Delta k_0)|=0$ and the central wavelength will disappear. Equation (15) shows that the variation of spectrum intensity of Δk_0 with the duty cycle D_m is linear. As the duty cycle D_m increases from 0 to 100%, $|F(\Delta k_0)|$ decreases linearly from $2\sin(\Delta k_0 a/2)/\pi$ (at $D_m=0$) to zero (at $D_m=50\%$), and then increases linearly from zero to $2\sin(\Delta k_0 a/2)/\pi$ (at $D_m=100\%$) as depicted by the dash-dotted curve in Fig. 7(a). It is also seen that although $|F(\Delta k_0)|$ will vary with the duty cycle D_0, the extinction of central wavelength is not dependent on it, except two extreme conditions $D_0=0$ (i.e., $a=0$) and 1 (i.e., $a=\Lambda_0$). It is seen that when $D_m=0$ or $D_m=100\%$, a CPOSL degenerates to a POSL. And from Eq. (15), the spectrum intensity of the central spectral component Δk_0 can be expressed by $|2\sin(\Delta k_0 a/2)/\pi|=|2\sin(\pi D_0)/\pi|$. It is obvious that in the conventional first-order QPM structure, the spectral intensity of Δk_0 varies with D_0 according to a sinusoid function. It

means that as D_0 changes, the spectrum intensity of Δk_0 in the first-order POSL can be smaller than that in the higher-order POSL (spectrum intensity Δk_0 in POSL can be expressed by $2/m\pi$, where m denotes the mth-order QPM condition). Only for $D_0=50\%$ can we obtain the maximum value of $\pi/2$ for a conventional POSL.

The spectrum intensities of the spectral components $\Delta k_1 = \Delta k_0 + \delta_{\Delta k}$ and $\Delta k_2 = \Delta k_0 - \delta_{\Delta k}$ ($|F(\Delta k_1)|$ and $|F(\Delta k_2)|$) can be expressed by

$$\left| \lim_{\Delta k \to \Delta k_1} F(\Delta k) \right| = \frac{8}{\Delta k_1 \Lambda_m} \left| \frac{\sin(\Delta k_1 a/2)}{\sin(\Delta k_1 \Lambda_0/2)} \sin(\Delta k_1 \Lambda_m D_m/2) \right|, \tag{16}$$

$$\left| \lim_{\Delta k \to \Delta k_2} F(\Delta k) \right| = \frac{8}{\Delta k_2 \Lambda_m} \left| \frac{\sin(\Delta k_2 a/2)}{\sin(\Delta k_2 \Lambda_0/2)} \sin(\Delta k_2 \Lambda_m D_m/2) \right|. \tag{17}$$

Distributions of $|F(\Delta k_1)|$ and $|F(\Delta k_2)|$ as a function of D_m are depicted by the solid and dashed curves in Fig. 7(a), respectively. From Eqs. (16) and (17), it is seen that the variations of $|F(\Delta k_1)|$ and $|F(\Delta k_2)|$ depend not only on D_m, but also on Λ_m. In the entire duty cycle range, both $|F(\Delta k_1)|$ and $|F(\Delta k_2)|$ beat with roughly equal amplitude (for $\delta_{\Delta_k} \ll \Delta k_0$) but different phases, and the beating frequency is proportional to Λ_m. Thus $|F(\Delta k_1)|$ and $|F(\Delta k_2)|$ can be equalized at a series of discrete values of D_m as indicated by the black circles in the inset of Fig. 7(a).

From Fig. 7, when D_m deviates from the 50% point, the central wavelength will not disappear and the spectrum intensities of $\Delta k_0, \Delta k_1$, and Δk_2 will vary as D_m. Thus one can further adjust all the spectral components to have equal intensities. However, instead of equating Eqs. (15), (16), and (17) directly, we use numerical iteration. $|F(\Delta k_0)|, |F(\Delta k_1)|$, and $|F(\Delta k_2)|$ can be roughly equalized at the maximum value around $D_m=0.262$, 0.275, 0.287 [Fig. 7(b)], or $D_m=(1-0.262)$, $(1-0.275)$, and $(1-0.287)$ [Fig. 7(c)]. Figure 6(c) shows a three-channel Fourier spectrum with almost equal spectrum intensities and Fig. 6(d) is a counterpart of Fig. 6(c) in the power spectrum. In brief, one can realize multiple-wavelength conversion with an arbitrary number of wavelength outputs by superimposing N different modulation periods with $D_m \neq 50\%$ on N equal segments.

V. CONCLUSIONS

In summary, we have systematically investigated the QPMM effect in the optical superlattices POSL, RPOSL, and CPOSL. Effective bandwidth enhancement is achieved by modulating the QPMM via the reset action in a RPOSL. Fourier analysis is adopted as an alternative approach for which small signal approximation is unavailable, and it is verified to be more general. Multiple-wavelength conversion is realized by modulating the QPMM via the cascaded action in a CPOSL. By studying the duty cycle of the modulation period, the CPOSL can be used to generate arbitrary numbers of wavelengths, even or odd numbers, rendering the CPOSL more suitable for practical applications.

ACKNOWLEDGMENT

This work is supported by the DSTA of Singapore under Grant No. POD0103451.

APPENDIX: DETERMINING THE PROPER POSITION OF THE RESET UNDER SMALL SIGNAL APPROXIMATION

Under the small signal approximation ($dE_p/dx=0$), the coupling equations can be analytically solved by a standard differential equation technique. The amplitude of the converted output is

$$E_{\text{out}}(L_{\text{sup}}) = \int_0^{L_{\text{sup}}} \frac{i\omega_{\text{out}} E_p E_s^*(x=0) d_{\text{eff}}}{2n_{\text{out}}c} f(x) \exp(i\Delta k x) dx. \tag{A1}$$

For example, for the RPOSL with only one reset superimposed, the integration in Eq. (A1) can be converted into the sum of integration of each single domain:

$$\begin{aligned} E_{\text{out}}^+(L_{\text{sup}}) &= \xi \left[\int_0^{\Lambda_0/2} d_{\text{eff}} \exp(i\Delta k x) dx + \cdots \right. \\ &\quad \left. + \int_{[L_{\text{sup}}/(\Lambda_0/2)-2]/\Lambda_0/2}^{[L_{\text{sup}}/(\Lambda_0/2)-1]\Lambda_0/2} d_{\text{eff}} \exp(i\Delta k x) dx \right] \\ &= \xi \sum_{m=0}^{L_{\text{sup}}/\Lambda_0-1} \int_{2m\Lambda_0/2}^{(2m+1)\Lambda_0/2} d_{\text{eff}} \exp(i\Delta k x) dx, \end{aligned}$$

$$\begin{aligned} E_{\text{out}}^-(L_{\text{sup}}) &= \xi \left[\int_{\Lambda_0/2}^{\Lambda_0} (-d_{\text{eff}}) \exp(i\Delta k x) dx + \cdots \right. \\ &\quad \left. + \int_{[L_{\text{sup}}/(\Lambda_0/2)-1]\Lambda_0/2}^{[L_{\text{sup}}/(\Lambda_0/2)]\Lambda_0/2} (-d_{\text{eff}}) \exp(i\Delta k x) dx \right] \\ &= \xi \sum_{m=0}^{L_{\text{sup}}/\Lambda_0-1} \int_{(2m+1)\Lambda_0/2}^{(2m+2)\Lambda_0/2} (-d_{\text{eff}}) \exp(i\Delta k x) dx, \end{aligned} \tag{A2}$$

where $\xi = i\omega_{\text{out}} E_p E_s^*(x=0)/2n_{\text{out}}c$ is a constant. "+" and "−" represent the nonlinear contributions from the positive and negative domains, respectively. It should be noted that the deduction above is based on the approximation that the nonlinear contribution from the domain that contains the reset is neglected and the entire superlattice is treated as a combination of two POSLs. This approximation is tenable since both L_1 and L_2 are much larger than the width of a single domain. Then including the additional phase mismatch $\delta_{\Delta k}$, the relationship between the output amplitude and the position of the reset can be expressed by

$$\begin{aligned} E_{\text{out}} &= E_{\text{out}}^+ + E_{\text{out}}^- \\ &= \xi d_{\text{eff}} \left[\sum_{m=0}^{L_1/\Lambda_0-1} \int_{2m\Lambda_0/2}^{(2m+1)\Lambda_0/2} \exp(i\Delta k_0 x) \exp(i\delta_{\Delta k} x) dx \right. \\ &\quad \left. - \sum_{m=0}^{L_1/\Lambda_0-1} \int_{(2m+1)\Lambda_0/2}^{(2m+2)\Lambda_0/2} \exp(i\Delta k_0 x) \exp(i\delta_{\Delta k} x) dx \right. \end{aligned}$$

$$+\sum_{m=L_1/\Lambda_0}^{L_{\mathrm{sup}}/\Lambda_0-1}\int_{(2m)\Lambda_0/2}^{(2m+1)\Lambda_0/2}\exp(i\Delta k_0 x)\exp(i\delta_{\Delta k}x)dx$$
$$-\sum_{m=L_1/\Lambda_0}^{L_{\mathrm{sup}}/\Lambda_0-1}\int_{(2m+1)\Lambda_0/2}^{(2m+2)\Lambda_0/2}\exp(i\Delta k_0 x)\exp(i\delta_{\Delta k}x)dx\Bigg]. \tag{A3}$$

After a series of deductions, we obtain

$$E_{\mathrm{out}}=\frac{i\xi d_{\mathrm{eff}}}{\Delta k}\left[\exp\left(i\delta_{\Delta k}\frac{\Lambda_0}{2}\right)+1\right]\left[\sum_{m=0}^{2L_1/\Lambda_0-1}\exp\left(i\delta_{\Delta k}m\frac{\Lambda_0}{2}\right)-\sum_{m=2L_1/\Lambda_0}^{2L_{\mathrm{sup}}/\Lambda_0-1}\exp\left(i\delta_{\Delta k}m\frac{\Lambda_0}{2}\right)\right]$$
$$=\frac{i\xi d_{\mathrm{eff}}}{\Delta k\Lambda_0/2}\left[\exp\left(i\delta_{\Delta k}\frac{\Lambda_0}{2}\right)+1\right]\left[\int_0^{L_1}\exp(i\delta_{\Delta k}x)dx-\int_{L_1}^{L_{\mathrm{sup}}}\exp(i\delta_{\Delta k}x)dx\right]. \tag{A4}$$

After integration and applying $P_{\mathrm{out}}\sim|E_{\mathrm{out}}|^2$, we finally obtain

$$P_{\mathrm{out}}\sim\frac{64\xi^2 d_{\mathrm{eff}}^2\cos^2(\delta_{\Delta k}\Lambda_0/4)}{(\delta_{\Delta k}\Delta k\Lambda_0)^2}\left[2\sin^2\left(\frac{\delta_{\Delta k}L_1}{2}\right)+2\sin^2\left(\frac{\delta_{\Delta k}(L_{\mathrm{sup}}-L_1)}{2}\right)-\sin^2\left(\frac{\delta_{\Delta k}L_{\mathrm{sup}}}{2}\right)\right]. \tag{A5}$$

The decision of the proper position of the reset also has to depend on the same numerical balance process as discussed in Sec. III. Comparing Eqs. (9) and (A5), it is seen that the Fourier spectrum is similar to the power spectrum, verifying the validity of adopting the Fourier analysis as an effective and general approach to studying the bandwidth problem in $\chi^{(2)}$-induced frequency conversion processes.

[1] M. Yamada, N. Nada, M. Saitoh, and K. Watanabe, Appl. Phys. Lett. **62**, 435 (1993).

[2] L. E. Myers, R. C. Eckardt, M. M. Fejer, R. L. Byer, W. R. Bosenberg, and J. W. Pierce, J. Opt. Soc. Am. B **12**, 2102 (1995).

[3] Shi-ning Zhu, Yong-yuan Zhu, Zhi-yong Zhang, Hong Shu, Hai-feng Wang, Jing-fen Hong, and Chuan-zhen Ge, J. Appl. Phys. **77**, 5481 (1995).

[4] W. P. Risk, and S. D. Lau, Appl. Phys. Lett. **69**, 3999 (1996).

[5] Minoru Taya, Matthew C. Bashaw, and M. M. Fejer, Opt. Lett. **21**, 857 (1996).

[6] Lawrence E. Myers and Walter R. Bosenberg, IEEE J. Quantum Electron. **33**, 1663 (1997)

[7] Shi-ning Zhu, Yong-yuan Zhu, and Nai-ben Ming, Science **278**, 843 (1997).

[8] H. C. Guo, Y. Q. Qin, Z. X. Shen, and S. H. Tang, J. Phys.: Condens. Matter **16**, 8465 (2004).

[9] Martin M. Ferjer, G. A. Magel, Dieter H. Jundt, and Robert L. Byer, IEEE J. Quantum Electron. **28**, 2631 (1992).

[10] M. A. Arbore, O. Marco, and M. M. Fejer, Opt. Lett. **22**, 865 (1997).

[11] L. E. Myers, R. C. Eckardt, M. M. Fejer, R. L. Byer, and W. R. Bosenberg, Opt. Lett. **21**, 591 (1996).

[12] M. H. Chou, K. R. Parameswaran, and M. M. Fejer, Opt. Lett. **22**, 1157 (1999).

[13] Yiqiang Qin, Silvia M. Pietralunga, and Mario Martinelli, J. Lightwave Technol. **19**, 1298 (2001).

[14] Yuzo Sasaki, Avetisyan Yuri, Kodo Kawase, and Hiromasa Ito, Appl. Phys. Lett. **81**, 3323 (2002).

[15] Yong-yuan Zhu and Nai-ben Ming, Phys. Rev. B **42**, 3676 (1990).

[16] Dieter H. Jundt, Opt. Lett. **22**, 1553 (1997).